

A Parabolic Model for the Dimple Potentials

Melike Çıbık Aydın¹, Haydar Uncu¹, Coşkun Deniz²

¹*Department of Physics, Adnan Menderes University, Aytepe, 09100, Aydın, Turkey,*

²*Department of Electronics Engineering,*

Adnan Menderes University, Aytepe, 09100, Aydın, Turkey

(Dated: August 30, 2018)

Abstract

We study truncated parabolic function and demonstrate that it is a representation of the Dirac δ function. We also show that the truncated parabolic function, used as a potential in the Schrödinger equation, has the same bound state spectrum, tunneling and reflection amplitudes with the Dirac δ potential as the width of the parabola approximates to zero. Dirac δ potential is used to model dimple potentials which are utilized to increase the phase-space density of a Bose-Einstein condensate in a harmonic trap. We show that harmonic trap with a δ function at the origin is a limit case of the harmonic trap with a symmetric truncated parabolic potential around the origin. Therefore, we propose that the truncated parabolic potential is a better candidate for modeling the dimple potentials.

Keywords: Truncated Parabolic Potential, Dirac δ function, Dimple Potential, JWKB Approximation

I. INTRODUCTION

The dimple potentials are used to increase the phase space density of the dilute Bose gases [1–6]. This increase gives rise to the the formation of a Bose-Einstein condensate (BEC) when the initial sample is just above the critical temperature. So, the dimple potentials provide a means of inducing condensation without cooling [4]. Moreover, the improvements in the trapping techniques of cold atoms made possible to realize Bose-Einstein condensates in low dimensions [7–11]. Thus, theoretical models of dimple potentials in one dimension have been studied in the literature [12, 13]. While some of these models utilize an inverse Gaussian function others adopt Dirac δ functions to describe dimple potentials. We will use a truncated parabolic potential $V(x) = -U_0(1 - x^2/a^2)$ for $x \leq |a|$ to model dimple potentials first proposed in Ref. [3] for three dimensions. However, in this study Ma et. al. used a numeric simulation to explain for both the loading process and the subsequent evaporative cooling from a dimple potential.

The advantage of the parabolic model compared to Gaussian model is that the Schrödinger equation for the truncated parabolic potential is analytically solvable, so one obtains the thermodynamic quantities of a weakly interacting Bose gas at least as a first approximation. Although the Schrödinger equation for Dirac δ potentials are also analytically solvable, one can not incorporate both the dimple depth and width together into these models. Only the multiplication of these quantities are used as the coupling coefficient of the Dirac δ potential [12]. In addition to this, Dirac δ models are only valid for tough and narrow dimples. However, experiments with relative wide dimples are also performed [4]. Therefore, the parabolic model which accommodates both dimple depth and width separately is more useful in describing dimple potentials.

As a special case of point interactions, Dirac δ potential has been taking interest for years. Atkinson and Crater investigated the effect of a Dirac δ to the bound states of various potentials in one dimension [14]. Several authors made further studies on this subject [15–17]. Bound states of arbitrary but finite number of Dirac δ shells in higher dimensions are also studied [18]. The resonances of potentials with several Dirac δ are examined by Gadella et. al. [19, 20]. In physical applications, Dirac δ potential is mainly used to describe short range effects. For example, Erkol et. al. used δ potential for modeling short range interactions in atomic and nuclear physics [21, 22]. Moreover it is shown that δ potentials

can also be used to find approximate solutions for tunneling and reflection amplitudes for different potentials [23].

In this study, we suggest that the truncated parabolic function $f_\delta(x) = 3/(4a)(1-x^2/a^2)$, for $|x| \leq a$ is a representation of the Dirac δ function. Moreover, since the Schrödinger equation of the truncated parabolic potential is analytically solvable, we are able to show that the bound state spectrum, tunneling and reflection coefficients of the truncated parabolic potential go to those of the Dirac δ potential as the width decreases while the depth increases. We also demonstrate that the spectrum of the harmonic trap with a truncated parabolic potential reduces to the spectrum of the harmonic potential with a Dirac δ function in the same limit. So, the truncated parabolic potential model of the dimple trap includes all the results obtained for the non-interacting Bose gases by the Dirac δ models for the dimple potential as a special case.

The paper is organized as follows: In section II, we present the solution of the Schrödinger equation for a harmonic trap with a truncated parabolic potential in one dimension and obtain eigenvalue equations and eigenfunctions, for the sake of completeness. In order to find the eigenvalues, the eigenvalue equations are solved numerically. In section III, we apply JWKB approximation to check the validity of numerically found eigenvalues. In section IV, we use the sudden perturbation theory to find the transition amplitudes from harmonic trap to the harmonic trap with a dimple described by a truncated parabolic potential. In section V, we show that the truncated parabolic function provides a representation of the Dirac δ function. Moreover, we also demonstrate that the spectrum, the reflection and transmission coefficients of this potential reduces to those of the Dirac δ potential as the width of the truncated parabolic potential goes to zero, when the depth times width is fixed. Finally, we conclude in Section VI.

II. HARMONIC TRAP WITH A PARABOLIC POTENTIAL

In this section, we obtain the eigenvalues and the eigenfunctions of the Hamiltonian

$$\hat{H} = \frac{\hat{P}^2}{2m} + V(\hat{X}) \quad (1)$$

in one dimension where the potential function is given as

$$V(x) = \begin{cases} \frac{1}{2}m\omega^2 x^2 & \text{for } |x| > a \\ \frac{1}{2}m\omega^2 x^2 - U_0 \left(1 - \frac{x^2}{a^2}\right) & \text{for } |x| \leq a. \end{cases} \quad (2)$$

Here $U_0 > 0$ and $a > 0$ represent the depth and the width of the truncated parabolic potential, respectively.

The time independent Schrödinger equation for this potential is

$$-\frac{\hbar^2}{2m} \frac{d^2\Psi(x)}{dx^2} + V(x)\Psi(x) = E\Psi(x), \quad (3)$$

where $V(x)$ is given in the Eq. (2). For $U_0 = 0$, the Hamiltonian reduces to the harmonic oscillator Hamiltonian whose eigenvalues are $E_n = (n + 1/2)\hbar\omega$, $n = 0, 1, 2, \dots$ and whose eigenfunctions are given in terms of the Hermite polynomials $H_n(\sqrt{m\omega/\hbar} x)$. However if $U_0 \neq 0$, the eigenvalues are no more $(n + 1/2)\hbar\omega$ and the eigenfunctions cannot be written in terms of the Hermite polynomials $H_n(\sqrt{m\omega/\hbar} x)$, $n = 0, 1, 2, \dots$ whose degrees are finite.

The time independent Schrödinger equation of the Hamiltonian in Eq. (1) whose potential term is given in Eq. (2) is different for $|x| > a$ and for $|x| \leq a$. For $|x| > a$ the Schrödinger equation reduces to

$$-\frac{\hbar^2}{2m} \frac{d^2\Psi(x)}{dx^2} + \frac{1}{2}m\omega^2 x^2 \Psi(x) = E\Psi(x). \quad (4)$$

Although the differential equation (4) is same as the time independent Schrödinger equation for the harmonic oscillator potential, the solutions for $|x| > a$ differ from harmonic oscillator solution because of the continuity conditions on the wave functions and their derivatives at the points $|x| = a$.

We continue by rewriting the Eq. (4) in terms of dimensionless variable

$$z = \left(\frac{m\omega}{\hbar}\right)^{1/2} x \quad (5)$$

as

$$\frac{d^2\Psi(z)}{dz^2} + (2\varepsilon - z^2) \Psi(z) = 0 \quad (6)$$

where $\varepsilon = E/(\hbar\omega)$. The general solutions of Eq.(6) can be written in terms of parabolic cylinder functions [24]:

$$\begin{aligned} D_\lambda(z) &= 2^\lambda e^{-z^2/2} \left\{ \Gamma\left(\frac{1}{2}\right) \frac{\Phi(-\lambda/2, 1/2; z^2)}{\Gamma(\frac{1-\lambda}{2})} + \Gamma\left(-\frac{1}{2}\right) z \frac{\Phi((1-\lambda)/2, 3/2; z^2)}{\Gamma(\frac{-\lambda}{2})} \right\} \\ D_\lambda(-z) &= 2^\lambda e^{-z^2/2} \left\{ \Gamma\left(\frac{1}{2}\right) \frac{\Phi(-\lambda/2, 1/2; z^2)}{\Gamma(\frac{1-\lambda}{2})} - \Gamma\left(-\frac{1}{2}\right) z \frac{\Phi((1-\lambda)/2, 3/2; z^2)}{\Gamma(\frac{-\lambda}{2})} \right\} \end{aligned} \quad (7)$$

where $\lambda = \varepsilon - 1/2$, $\Gamma(x)$ is the well known gamma function and $\Phi(\alpha, \gamma; y)$ is the confluent hypergeometric function [24]. The asymptotic behavior of $D_\lambda(z)$ and $D_\lambda(-z)$ are as follows:

$$\lim_{z \rightarrow \infty} D_\lambda(z) = 0, \quad \lim_{z \rightarrow \infty} D_\lambda(-z) = \infty \quad \text{and} \quad \lim_{z \rightarrow -\infty} D_\lambda(-z) = 0, \quad \lim_{z \rightarrow -\infty} D_\lambda(z) = \infty.$$

Because $D_\lambda(\mp z)$ diverge at $\pm\infty$, the wave functions for $x < -a$ ($z < -(\frac{m\omega}{\hbar})^{1/2}a$) and $x > a$ ($z > (\frac{m\omega}{\hbar})^{1/2}a$) are

$$\psi_1(z) = c_1 D_\lambda(-z) \tag{8}$$

$$\psi_3(z) = c_4 D_\lambda(z) \tag{9}$$

where c_1 and c_4 are constants that can be determined by the normalization and continuity conditions.

For $|x| \leq a$, Eq. (3) takes the form

$$-\frac{\hbar^2}{2m} \frac{d^2\Psi(x)}{dx^2} + \left[\frac{1}{2}m\omega^2 x^2 - U_0 \left(1 - \frac{x^2}{a^2} \right) \right] \Psi(x) = E\Psi(x). \tag{10}$$

Defining

$$\omega_d = \sqrt{\omega^2 + \frac{2U_0}{ma^2}}, \quad \frac{E + U_0}{\hbar\omega_d} = \varepsilon_d, \quad \lambda_d = \varepsilon_d - \frac{1}{2} \tag{11}$$

and changing the variable to $z_d = \sqrt{\frac{m\omega_d}{\hbar}} x$, Eq. (10) takes a similar form with the Eq. (6):

$$\frac{d^2\Psi(z_d)}{dz_d^2} + (2\varepsilon_d - z_d^2) \Psi(z_d) = 0. \tag{12}$$

Therefore the solutions of this equation are same as Eq. (7) with z replaced by z_d and λ replaced by λ_d . Hence, the wave functions for $|x| \leq a$ are

$$\psi_2(z) = c_2 D_{\lambda_d}(z_d) + c_3 D_{\lambda_d}(-z_d) \tag{13}$$

where c_2 and c_3 are constants which can be found by normalization and continuity conditions. Since the potential is an even function of x , the eigenfunctions are either even or odd (hence $c_4 = \pm c_1$ in Eq. (9) and $c_3 = \pm c_2$ in Eq. (13)):

$$\Psi_\lambda(z) = \begin{cases} c_1 D_\lambda(-z) & \text{for } z < -(\frac{m\omega}{\hbar})^{1/2}a \\ c_2 [D_{\lambda_d}(z_d) \pm D_{\lambda_d}(-z_d)] & \text{for } |z| < (\frac{m\omega}{\hbar})^{1/2}a \\ \pm c_1 D_\lambda(z) & \text{for } z > (\frac{m\omega}{\hbar})^{1/2}a \end{cases} \tag{14}$$

where $+$ and $-$ signs stand for the even and odd eigenfunctions in the second and third regions of the wave functions in Eq. (14). Applying the continuity conditions on the wave functions and their derivatives, at $|x| = a$, one can express c_2 in terms of c_1 and get equations which determine the eigenvalues of the Hamiltonian for the even and odd eigenfunctions, respectively:

$$\sqrt{\frac{\omega}{\omega_d}} [D_{\lambda_d}(B) + D_{\lambda_d}(-B)] G_\lambda(A) = [G_{\lambda_d}(B) - G_{\lambda_d}(-B)] D_\lambda(A) \quad (15)$$

$$\sqrt{\frac{\omega}{\omega_d}} [D_{\lambda_d}(B) - D_{\lambda_d}(-B)] G_\lambda(A) = [G_{\lambda_d}(B) + G_{\lambda_d}(-B)] D_\lambda(A) \quad (16)$$

for $D_\lambda(A) \neq 0$ and $G_\lambda(A) \neq 0$,

where

$$G_\lambda(z) = \frac{d}{dz} D_\lambda(z), \quad (17)$$

and $A = \sqrt{\frac{m\omega}{\hbar}} a$, $B = \sqrt{\frac{m\omega_d}{\hbar}} a$.

The Eqs. (15) and (16), corresponding to the even and odd eigenfunctions respectively, have infinite number of roots and can be solved numerically to determine λ and therefore the eigenvalues $E_\lambda = (\lambda + 1/2)\hbar\omega$.

III. JWKB APPROXIMATION

In the previous section we obtained analytically the eigenvalue Eqs. (15), (16) and the eigenfunctions of the Hamiltonian in Eq. (1) whose potential term is given in Eq. (2). However, to determine the eigenvalues one needs to solve the Eqs. (15) and (16) numerically [33]. As U_0 i.e. the depth of the potential increases, the eigenvalues of the low lying states decrease. As the eigenvalues decrease one needs to check the accuracy of the values obtained by numerical methods. For this aim we apply JWKB [34] approximation because it gives the exact eigenvalues [26–29] for harmonic oscillator Hamiltonian whose potential term is one of the shape invariant potentials [27].

The JWKB approximation method gives rise to the well known JWKB quantization formula to find the eigenenergies (e.g. see [29]),

$$\int_{x_1}^{x_2} [2m(E_n - V(x))]^{1/2} dx = (n + \frac{1}{2})\hbar \quad (18)$$

where x_1 and x_2 are classical turning points found by the equality $E_n = V(x_{1,2})$. Since the potential function is different for $|x| \leq a$ and $|x| > a$ the quantization formula differs for

$E_n < (1/2)m\omega^2 a^2$ and for $E_n > (1/2)m\omega^2 a^2$. We will denote the eigenenergies whose values are less than $V(a) = (1/2)m\omega^2 a^2$ by $E_n^{(1)}$. For these eigenenergies, Eq. (18) becomes

$$\begin{aligned} \int_{x_1}^{x_2} [2m(E_n^{(1)} - V(x))]^{1/2} dx &= \int_{x_1}^{x_2} \sqrt{2m \left[E_n^{(1)} - \left(\frac{1}{2}m\omega^2 x^2 - U_0 \left(1 - \frac{x^2}{a^2}\right) \right) \right]} dx = \\ \int_{x_1}^{x_2} \sqrt{2m \left[E_n^{(1)} + U_0 - \left(\frac{1}{2}m\omega_d^2 x^2 \right) \right]} dx &= \left(n + \frac{1}{2}\right)\hbar\pi \end{aligned} \quad (19)$$

where ω_d is defined in Eq. (11) and $x_{1,2} = \pm\sqrt{(2E_n^{(1)} + U_0)/(m\omega_d^2)}$. It is easy to solve Eq. (19) for $E_n^{(1)}$:

$$E_n^{(1)} = -U_0 + \left(n + \frac{1}{2}\right)\hbar\omega_d \quad \text{for } n = 0, 1, \dots, n' - 1 \quad . \quad (20)$$

Here, (n') is the number of the eigenstates whose eigenvalues are less than $V(a)$. It is necessary to determine the lowest level index for the eigenstates in the upperlying region whose eigenvalues are larger than $V(a)$ (See Eq. (22)). n' is determined by the formula

$$n' = \left\lfloor \frac{\frac{1}{2}m\omega^2 a^2 - E_0^{(1)}}{\hbar\omega_d} \right\rfloor + 1, \quad (21)$$

where the brackets denote the floor function. The JWKB quantization equation (18) for the energy eigenvalues of the eigenstates in the upperlying region becomes

$$\begin{aligned} 2 \left\{ \int_0^a \sqrt{2m \left[E_n^{(2)} + U_0 - \left(\frac{1}{2}m\omega_d^2 x^2 \right) \right]} dx + \int_a^{x_2} \sqrt{2m \left(E_n^{(2)} - \frac{1}{2}m\omega^2 x^2 \right)} dx \right\} \\ = \left(n + \frac{1}{2}\right)\hbar\pi \quad \text{for } n = n', n' + 1, \dots, \end{aligned} \quad (22)$$

where $x_2 = \sqrt{(2E)/m\omega^2}$ and n' is given by Eq. (21). We take the integrals in Eq. (22) only for positive values of x utilizing the fact that the potential function is an even function. After taking the integrals the JWKB quantization equation for $E_n^{(2)} > V(a)$ gives

$$\begin{aligned} \frac{2(E_n^{(2)} + U_0)}{\omega_d} \arcsin \left[\frac{a}{\sqrt{\frac{2(E_n^{(2)} + U_0)}{m\omega_d^2}}} \right] + ma\omega_d \sqrt{\frac{2(E_n^{(2)} + U_0)}{m\omega_d^2} - a^2} \\ = \frac{E_n^{(2)}}{\omega} \left\{ \pi - 2 \arcsin \left[\frac{a}{\sqrt{\frac{2E_n^{(2)}}{m\omega^2}}} \right] \right\} - ma\omega \sqrt{\frac{2E_n^{(2)}}{m\omega^2} - a^2} = \left(n + \frac{1}{2}\right)\hbar\pi. \end{aligned} \quad (23)$$

This equation also can be solved only numerically like Eq. (15) and (16). However its solution is much easier than the Eq. (15) and (16) in which one has to find the roots of infinite series.

TABLE I: The eigenenergies of the first few eigenstates for $\hbar = 1$, $m = 1/2$, $\omega = 1$, $a = 3$, $U_0 = 10$. For these values $n' = 5$ and $V(a) = 2.25$. All the energies are in units of $\hbar\omega$.

The Eigenenergies				
	The Eigenstate No	Analytic	JWKB	Difference Analytic-JWKB
$E_n^{(1)}$	0	-8.8333	-8.8333	0.0000
	1	-6.5001	-6.5000	0.0001
	2	-4.1681	-4.1667	0.0014
	3	-1.8447	-1.8333	0.114
	4	0.4355	0.5000	0.0645
$E_n^{(2)}$	5	2.5432	2.6852	0.1420
	6	4.1711	4.0504	0.1207
	7	5.2756	5.2638	0.0118
	8	6.3845	6.4181	0.0336
	9	7.5823	7.5390	0.0433
	10	8.6277	8.6381	0.1040
	11	9.7171	9.7217	0.0046

We compare the values of the eigenenergies obtained by the JWKB approximation and those found by the numerical solutions of the Eqs. (15) and (16) for different U_0 and a values in the Tables I and II. In the Table I, we take $\hbar = 1$, $2m = 1$. In the Table II (at the end of the manuscript), we take the true value for \hbar and more realistic values for the other parameters [30]. In these tables the first n' eigenenergies, denoted by $E_n^{(1)}$, are less than $V(a)$, and their JWKB values are calculated by the Eq. (20) and $E_n^{(2)}$ s are larger than $V(a)$ and their JWKB values are calculated by Eq. (23).

The potential energy function given in Eq. (2) changes its form at $|x| = a$ where its value is $V(a)$. Unless the eigenenergies are close to this value, the JWKB approximation gives accurate results. However, as the values of the eigenenergies get close to the $V(a)$, the accuracy of the JWKB approximation decreases. It is still useful to apply JWKB approximation in this interval because in numerical calculations one may skip some of the eigenstates since the difference between the successive eigenvalues are not uniform in this interval. The reason that the JWKB approximation gives accurate results for the ground

and first few excited eigenstates but not for the eigenstates whose eigenenergy values are around $V(a)$ is the following: The eigenfunctions of the ground and first few excited states go to zero very rapidly as $|x|$ increases and they are almost zero at $|x| = a$. So these eigenfunctions behave like they are the eigenfunctions of the shifted harmonic oscillator potential $V(x) = -U_0 + (1/2) m\omega_d^2 x^2$ for which the JWKB approximation gives exact results. In other words they don't "feel" the change of the form of the potential. For the excited states whose eigenvalues are much larger than $V(a)$, the JWKB approximation becomes again accurate. We can explain this also using the eigenfunctions of these states. These eigenfunctions are nonzero up to very large values compared to $|x| = a$. So the region where the dimple potential exists $|x| \leq a$ is very narrow compared to the width of these eigenfunctions. Therefore, they are not much effected by the dimple potential.

IV. TRANSITION AMPLITUDES

In a recent paper, Garrett et. al. report the formation of a Bose-Einstein condensate without cooling in an anisotropic harmonic trap using dimple potentials [4]. In this study, they investigate the behavior of a Bose gas in a harmonic trap with "narrow" and "wide" dimples both for adiabatic and sudden processes. For the sudden turn of the dimple, the sudden perturbation theory can be used to calculate the condensate fraction. By describing the harmonic trap with a dimple potential by Eq. (2), it is possible to apply sudden perturbation theory since one can calculate the eigenfunctions for both case (only harmonic trap $V(x) = (1/2) m\omega^2 x^2$ for $-\infty < x < \infty$ and harmonic trap with a dimple potential).

In this section, we will present the sudden perturbation calculations for one dimensional case. Before the turn on of the dimple, the potential is only the harmonic potential and the eigenfunctions for this case are [28, 29]:

$$\psi_n(z) = \left(\frac{(m\omega)^{1/2}}{(\pi\hbar)^{1/2} 2^n n!} \right)^{1/2} \exp(-z^2/2) H_n(z), \quad (24)$$

where z is given by Eq. (5). The eigenfunctions of the potential given by Eq. (2) are found in Section II and given in Eq. (14). Using the sudden perturbation theory [28], we calculate the transition amplitudes as

$$t_{n\lambda}(z) = \sqrt{\frac{\hbar}{m\omega}} \int_{-\infty}^{\infty} \psi_n(z) \Psi_\lambda(z) dz. \quad (25)$$

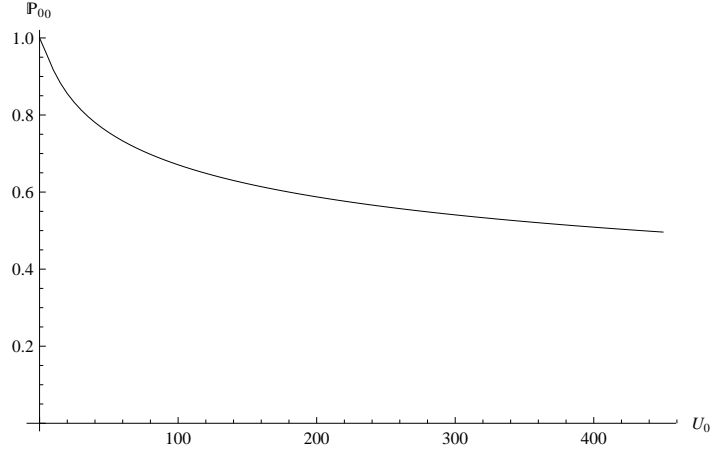


FIG. 1: The change of the transition probability from the ground state of the harmonic oscillator Hamiltonian to the ground state of the harmonic oscillator with a dimple potential \mathbb{P}_{00} with respect to the depth of the dimple U_0 .

In this equation one has to choose c_1 in Eq. (14) such that $\Psi_\lambda(z)$ is normalized to unity to find the transition probabilities as:

$$P_{n\lambda} = |t_{n\lambda}|^2. \quad (26)$$

We present the change of the transition probabilities with respect to U_0 from the ground state and from the second excited state of the harmonic oscillator to the ground state of

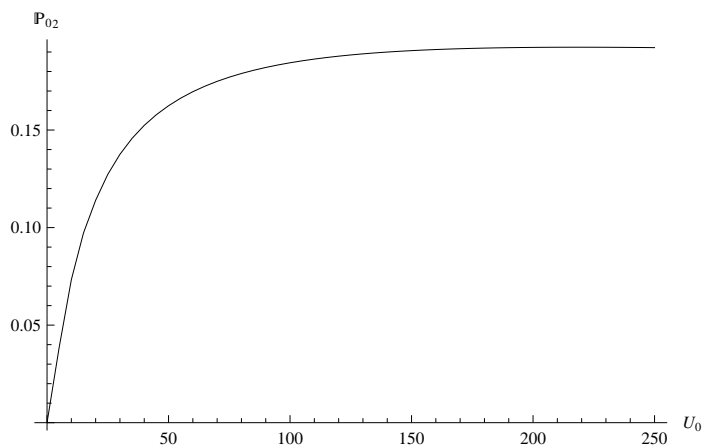


FIG. 2: The change of the transition probability from the second excited state of the harmonic oscillator Hamiltonian to the ground state of the harmonic oscillator with a dimple potential \mathbb{P}_{02} with respect to the depth of the dimple U_0 .

the harmonic oscillator with a dimple for the values $\hbar = 1$, $m = 1/2$, $\omega = 1$, $a = 3$ in the Figures 1 and 2, respectively. The transitions from the even eigenstates to odd eigenstates are zero since the wave functions of these states are even and odd functions.

In following studies we aim to use the truncated parabolic potential to model dimple potentials used in Bose Einstein condensation experiments. Similar transition probability calculations from higher levels to the new ground state can be used for the calculation of the condensate fraction of a BEC in a harmonic trap with a dimple when the dimple is turned on suddenly [4].

V. DIRAC δ POTENTIAL AS A LIMITING CASE OF THE PARABOLIC POTENTIAL

Recent papers show that modeling dimple potentials by Dirac δ functions reveal basic properties of a BEC in a harmonic trap with a dimple [12, 13]. In this section we will present that the δ potential is included in the truncated parabolic potential as a special case.

We will first show that the function

$$f_\delta(x) = \begin{cases} \frac{3}{4a} \left(1 - \frac{x^2}{a^2}\right) & \text{for } |x| \leq a \\ 0 & \text{for } |x| > a \end{cases} \quad (27)$$

represents the Dirac δ function. There is an advantage of this representation compared to other representations in the literature (see e.g. [31] Appendix II). When the function $f_\delta(x)$ in Eq. (27) is used as a potential for a Hamiltonian like in Eq. (2), the resulting time-independent Schrödinger equation is analytically solvable.

It is clear that the representation given in Eq. (27) satisfies the condition $\int_{-\infty}^{\infty} \delta(x)dx = 1$ used in defining Dirac δ function. We will show that this definition satisfies also the sampling property of δ function [32]: $\int_{-\infty}^{\infty} \delta(x)h(x)dx = h(0)$ for $a \rightarrow 0$ where $h(x)$ denotes an analytical function. That is

$$\lim_{a \rightarrow 0} \int_{-\infty}^{\infty} f_\delta(x)h(x)dx = \lim_{a \rightarrow 0} \int_{-a}^a f_\delta(x)h(x)dx = h(0). \quad (28)$$

For this aim we define the functions $H_1(x)$, $H_2(x)$, $H_3(x)$ as [35]

$$\frac{dH_1(x)}{dx} = h(x), \quad \frac{d^2H_2(x)}{dx^2} = h(x) \quad \frac{d^3H_3(x)}{dx^3} = h(x). \quad (29)$$

We apply three times integration by parts to the expression $\lim_{a \rightarrow 0} \int_{-a}^a f_\delta(x)h(x)dx$ and get

$$\lim_{a \rightarrow 0} \int_{-a}^a f_\delta(x)h(x)dx = \lim_{a \rightarrow 0} \left\{ \frac{3}{2a^2} [H_2(a) + H_2(-a)] - [H_3(a) - H_3(-a)] \right\}. \quad (30)$$

Using the Maclaurin series expansion of $H_2(a)$, $H_2(-a)$ and $H_3(a)$, $H_3(-a)$ up to a^3 one can see that the right hand side of the Eq. (30) is equal to $h(0)$ in the limit $a \rightarrow 0$.

It is well known that there is only one bound state of the Dirac delta potential (see e.g. [18])

$$V_\delta = -\frac{\hbar^2}{2m} \sigma \delta(x). \quad (31)$$

The solution of the eigenvalue equation for this potential is $\kappa = \sigma/2$ where $\kappa = \sqrt{-(2mE)}/\hbar$. Therefore one finds [18]

$$E = -\frac{\hbar^2 \sigma^2}{8m}. \quad (32)$$

Here the coupling coefficient of the δ function is taken as $-\hbar^2 \sigma/(2m)$ for calculational convenience. We will now calculate the bound state eigenvalues for the potential

$$V(x) = \begin{cases} -U_0 \left(1 - \frac{x^2}{a^2}\right) & \text{for } |x| \leq a \\ 0 & \text{for } |x| > a \end{cases} \quad (33)$$

and present that for small a the eigenvalue of the ground state energy of this potential approximates to the ground state energy of Dirac δ potential given in Eq. (31). The even and odd eigenfunctions of the bound states for the potential given in Eq. (33) is:

$$\psi_e(x) = \begin{cases} A_e e^{\kappa x} & \text{for } x < -a \\ B_e [D_{\gamma_d}(\sqrt{\frac{m\nu}{\hbar}}x) + D_{\gamma_d}(-\sqrt{\frac{m\nu}{\hbar}}x)] & \text{for } |x| \leq a \\ A_e e^{-\kappa x} & \text{for } x > a \end{cases} \quad (34)$$

and

$$\psi_o(x) = \begin{cases} A_o e^{\kappa x} & \text{for } x < -a \\ B_o [D_{\gamma_d}(\sqrt{\frac{m\nu}{\hbar}}x) - D_{\gamma_d}(-\sqrt{\frac{m\nu}{\hbar}}x)] & \text{for } |x| \leq a \\ -A_o e^{-\kappa x} & \text{for } x > a \end{cases} \quad (35)$$

where $\nu = \sqrt{2U_0/(ma^2)}$, $\gamma_d = (E + U_0)/(\hbar\nu) - 1/2$ and the coefficients A_e , A_o , B_e and B_o are to be determined from normalization and continuity conditions of the wave function and

its derivative. Applying these continuity conditions one gets the eigenvalue equation for the potential given in Eq. (33) of the even and odd eigenfunctions, respectively as:

$$-\kappa\sqrt{\frac{\hbar}{m\nu}} = -\sqrt{-(2\gamma+1)} = \frac{G_{\gamma_d}(\sqrt{\frac{m\nu}{\hbar}}a) - G_{\gamma_d}(-\sqrt{\frac{m\nu}{\hbar}}a)}{D_{\gamma_d}(\sqrt{\frac{m\nu}{\hbar}}a) + D_{\gamma_d}(-\sqrt{\frac{m\nu}{\hbar}}a)} \quad (36)$$

$$-\kappa\sqrt{\frac{\hbar}{m\nu}} = -\sqrt{-(2\gamma+1)} = \frac{G_{\gamma_d}(\sqrt{\frac{m\nu}{\hbar}}a) + G_{\gamma_d}(-\sqrt{\frac{m\nu}{\hbar}}a)}{D_{\gamma_d}(\sqrt{\frac{m\nu}{\hbar}}a) - D_{\gamma_d}(-\sqrt{\frac{m\nu}{\hbar}}a)} \quad (37)$$

where $\gamma = E/(\hbar\nu) - 1/2$; $D_\lambda(z)$ and $G_\lambda(z)$ are defined in Eqs. (7) and (17), respectively. By taking into account the definition of the representation for δ in Eq. (27), the comparison of Eqs. (31) and (33) reveals that $\sigma = 8maU_0/(3\hbar^2)$. As $a \rightarrow 0$, for constant U_0a , the eigenvalue Eq. (36) reduces to the Eq. (32) which gives the bound state eigenvalue of the δ potential. One can show this by expanding the right hand side of the Eq. (36) into a Taylor series. For constant U_0a , the left hand side of the equality in Eq. (36) is order of $a^{3/4}$ [36]. Therefore, we expand the right hand side in terms of $\sqrt{m\nu/\hbar}a$ so that the expansion terms in the right hand side include terms up to $a^{3/4}$. Doing this, we get the equality

$$-\sqrt{-(2\gamma+1)} = -(2\gamma_d+1)\sqrt{\frac{m\nu}{\hbar}}a + \frac{7}{6}\left(\sqrt{\frac{m\nu}{\hbar}}a\right)^3. \quad (38)$$

Substituting $\nu = \sqrt{2U_0/(ma^2)}$, $\gamma_d = (E + U_0)/(\hbar\nu) - 1/2$ and $\gamma = E/(\hbar\nu) - 1/2$ into this equation we find

$$E = -\frac{8mU_0^2a^2}{9\hbar^2}. \quad (39)$$

Since $\sigma = 8maU_0/(3\hbar^2)$, Eq. (39) is identical to the Eq. (32), which reveals that as $a \rightarrow 0$ the representation given in Eq. (27) gives the same ground state eigenvalue with δ potential for the solution of the Schrödinger equation. Doing a similar expansion to the Eq. (37), we see that this equation does not have a solution in the limit $a \rightarrow 0$. That means there is no odd bound state which proves there is only one bound state for the potential given in Eq. (33) in the limit $a \rightarrow 0$.

We also calculate the reflection and tunneling probabilities for the truncated parabolic potential given in Eq. (33) for the scattering states. Then, we show that as $a \rightarrow 0$, the tunneling and reflection amplitudes for this potential reduce to the transition and reflection amplitudes for the Dirac δ potential given in Eq. (31). The wave function for a scattering state of a δ potential incoming from $-\infty$ with an energy $E > 0$ can be written as:

$$\psi_{\delta s}(x) = \begin{cases} e^{ikax} + R_\delta e^{-ikax} & \text{for } x < -a \\ T_\delta e^{ikax} & \text{for } x > a \end{cases} \quad (40)$$

where $k = \sqrt{2mE/\hbar^2}$ and we take the coefficient of the wave incoming from $-\infty$ equal to unity for calculational convenience. The transition and reflection amplitudes for this potential is easily found to be

$$T_\delta = \frac{2ik}{2ik + \sigma} \quad (41)$$

$$R_\delta = -\frac{\sigma}{2ik + \sigma}. \quad (42)$$

The wave function for a scattering state incoming from $-\infty$ with an energy $E > 0$ for the potential in Eq. (33) can be written as:

$$\psi_s(x) = \begin{cases} e^{ikax} + Re^{-ikax} & \text{for } x < -a \\ c_1 D_{\gamma_d}(\sqrt{\frac{mE}{\hbar}}x) + c_2 D_{\gamma_d}(-\sqrt{\frac{mE}{\hbar}}x) & \text{for } |x| \leq a \\ Te^{ikax} & \text{for } x > a. \end{cases} \quad (43)$$

The norm squares of R and T given in Eq. (43) give the probability of reflection and tunneling, respectively. These coefficients are calculated using the continuity of the wave function and its derivative at points $x = |a|$. In order to present the result for R , we define

$$F_1(\lambda, a) = -\Phi\left(-\frac{\lambda}{2}, \frac{1}{2}, a^2 s^2\right) + 2(1 + \lambda)\Phi\left(-\frac{\lambda}{2}, \frac{3}{2}, a^2 s^2\right) \quad (44)$$

$$F_2(\lambda, a) = (k^2 + s^2 + a^2 s^4) \Phi\left(-\frac{\lambda}{2}, \frac{1}{2}, a^2 s^2\right) - 2s^2(1 + a^2 s^2)(1 + \lambda)\Phi\left(-\frac{\lambda}{2}, \frac{3}{2}, a^2 s^2\right) \quad (45)$$

$$F_3(\lambda, a) = 3(-1 + iak + a^2 s^2) \Phi\left(\frac{1-\lambda}{2}, \frac{3}{2}, a^2 s^2\right) + 2a^2 s^2(-1 + \lambda)\Phi\left(\frac{3-\lambda}{2}, \frac{5}{2}, a^2 s^2\right) \quad (46)$$

$$F_4(\lambda, a) = 2as^2\lambda\Phi\left(1 - \frac{\lambda}{2}, \frac{3}{2}, a^2 s^2\right) + (ik + as^2)\Phi\left(-\frac{\lambda}{2}, \frac{1}{2}, a^2 s^2\right), \quad (47)$$

where $\Phi(\alpha, \gamma; y)$ is the confluent hypergeometric function [24]. In terms of the functions $F_1(\lambda, a)$ to $F_4(\lambda, a)$ the reflection amplitude is

$$R = -\frac{ae^{-2iak} [2a^2 s^4(2 + \lambda)\Phi\left(\frac{1-\lambda}{2}, \frac{5}{2}, a^2 s^2\right) F_1(\lambda, a) + 3\Phi\left(\frac{1-\lambda}{2}, \frac{3}{2}, a^2 s^2\right) F_2(\lambda, a)]}{F_3(\lambda, a) F_4(\lambda, a)}. \quad (48)$$

In order to demonstrate T , we additionally define

$$F_5(\lambda, a) = -2a^2 s^2(2 + \lambda)\Phi\left(\frac{1}{2} - \frac{\lambda}{2}, \frac{5}{2}, a^2 s^2\right) \Phi\left(-\frac{\lambda}{2}, \frac{1}{2}, a^2 s^2\right) \quad (49)$$

$$F_6(\lambda, a) = \Phi\left(-\frac{\lambda}{2}, \frac{1}{2}, a^2 s^2\right) + 2a^2 s^2(1 + \lambda)\Phi\left(-\frac{\lambda}{2}, \frac{3}{2}, a^2 s^2\right). \quad (50)$$

In terms of the functions $F_3(\lambda, a)$ to $F_6(\lambda, a)$

$$T = -\frac{ie^{-2iak}k [F_5(\lambda, a) + 3\Phi(\frac{1-\lambda}{2}, \frac{3}{2}, a^2s^2) F_6(\lambda, a)]}{F_3(\lambda, a) F_4(\lambda, a)}. \quad (51)$$

In the appendix, we show the change of the tunneling and reflection probabilities with respect to energy E , width a and depth U_0 of the truncated parabolic potential. Now we will show that the tunneling amplitude T for the potential given in Eq. (33) goes to T_δ in Eq. (41). For this reason assuming U_0a is constant, we expand the numerator and the denominator of the right hand side of the Eq. (51) with respect to a and since we are interested in the limit $a \rightarrow 0$, we keep only the constant terms which are independent of a . Doing this, we find

$$\lim_{a \rightarrow 0} T = \frac{3ik}{3ik + 4mU_0a/\hbar^2}. \quad (52)$$

Since $\sigma = 8maU_0/(3\hbar^2)$, we see that T reduces to T_δ given in Eq. (41) for constant U_0a .

Finally, we show that the eigenvalues of the Hamiltonian with the potential given in Eq. (2) approximates to the eigenvalues of the Hamiltonian with the potential

$$V(x) = \frac{1}{2}m\omega^2x^2 - \frac{\hbar^2}{2m}\sigma\delta(x) \quad (53)$$

for $U_0 = 3\hbar^2\sigma/(8ma)$ as $a \rightarrow 0$. The eigenvalues of even states of the Hamiltonian with the potential of the Eq. (53) is equal to $E_\lambda = (\lambda + 1/2)\hbar\omega$ where λ values are the roots of the equation [12, 15]

$$\frac{\Gamma(\frac{1-\lambda}{2})}{\Gamma(-\frac{\lambda}{2})} = \frac{\Lambda}{4}. \quad (54)$$

Here $\Lambda = \sigma\sqrt{\hbar/(m\omega)}$. The odd eigenvalues are equal to the odd eigenvalues of the harmonic oscillator potential i.e. they are equal to $E_n = (n + 1/2)\hbar\omega$ for $n = 1, 3, 5, \dots$ [12]. As $a \rightarrow 0$, for constant $U_0a = c$, Eq. (15) reduces to Eq. (54) and the roots λ of Eq. (16) go to $\lambda_n = 2n + 1$ where $n = 0, 1, 2, 3, \dots$. In order to show this, we first expand $\sqrt{\omega/\omega_d}$ with respect to a and find

$$\sqrt{\frac{\omega}{\omega_d}} = \left(\frac{ma^3\omega^2}{2c}\right)^{1/4} \left(1 + \frac{ma^3\omega^2}{2c}\right)^{-1/4} \approx \left(\frac{ma^3\omega^2}{2c}\right)^{1/4} \left(1 - \frac{1}{4}\frac{ma^3\omega^2}{2c} + O(a^3)\right) \quad (55)$$

for $U_0a = c$. Then we expand $D_{\lambda_d}(B)$, $D_{\lambda_d}(-B)$, $G_{\lambda_d}(B)$, $G_{\lambda_d}(-B)$ in terms of $B = \sqrt{m\omega_d/\hbar}a$; $G_\lambda(A)$ and $D_\lambda(A)$ in terms of $A = \sqrt{m\omega/\hbar}a$ in Eq. (15) and obtain for the eigenvalue equation of the even eigenfunctions

$$-\frac{8}{3} \frac{(\Gamma(1/2))^2}{\Gamma(\frac{1-\lambda_d}{2})\Gamma(\frac{1-\lambda}{2})} \frac{(mc)^{3/4}}{2^{1/4}\hbar^{3/2}} a^{3/4} = 2 \left(\frac{m}{2c}\right)^{1/4} \omega^{1/2} \frac{\Gamma(1/2)\Gamma(-1/2)}{\Gamma(\frac{1-\lambda_d}{2})\Gamma(-\frac{\lambda}{2})} a^{3/4}. \quad (56)$$

After rearranging the terms we get

$$\frac{2}{3} \frac{U_0 a m^{1/2}}{\hbar^{3/2} \omega^{1/2}} = \frac{\Gamma(\frac{1-\lambda}{2})}{\Gamma(-\frac{\lambda}{2})}. \quad (57)$$

When we insert $\sigma = 8maU_0/(3\hbar^2)$ and $\Lambda = \sigma\sqrt{\hbar/(m\omega)}$ into Eq. (57), we see that this equation reduces to the Eq. (54). Applying a similar procedure to the eigenvalue Eq. (16) of the odd eigenfunctions, we see that it reduces to

$$\frac{\Gamma(-1/2)\Gamma(1/2)}{\Gamma(\frac{1-\lambda_d}{2})\Gamma(-\frac{\lambda_d}{2})} = 0 \quad (58)$$

as $a \rightarrow 0$ for constant U_0a . In this limit $\lambda_d = -1/2$, therefore the right hand side of Eq. (58) can be equal to zero if and only if $\Gamma(\frac{1-\lambda}{2}) = \infty$. Since $\Gamma(-n) = \infty$ when $n = 0, 1, 2, \dots$, we get for λ

$$\frac{1-\lambda}{2} = -n \quad \Rightarrow \quad \lambda = 2n + 1 \quad \text{for } n = 0, 1, 2, \dots. \quad (59)$$

Therefore, similar to the Dirac δ case, in the limit $a \rightarrow 0$ the odd eigenvalues of the potential given in Eq. (2) reduces to the odd eigenvalues of the harmonic oscillator potential with a Dirac δ potential at the origin.

The fact that the eigenvalues of the harmonic potential with a symmetric truncated parabolic potential around the origin reduce to the eigenvalues of the harmonic potential with a Dirac δ at the origin, in the limit $a \rightarrow 0$ for fixed U_0a , shows that the results obtained modeling the dimple potential with a Dirac δ for a non-interacting BEC in a harmonic trap with a dimple [12, 13] is included in the parabolic model of the dimple as a special case.

VI. CONCLUSION

We propose, in this study, that the parabolic potential defined in Eq. (2) is more appropriate for modeling the dimple potentials than the Dirac δ potential used in the literature. Therefore, we showed that the parabolic potential includes the Dirac δ potential as a special case and the wave functions, eigenvalues, tunneling and reflection coefficients of the Dirac δ potential can be obtained from those of the parabolic potential as a limiting case.

In section II, we have summarized the solution of the Schrödinger equation for a harmonic trap with a truncated parabolic potential in one dimension and obtained eigenvalue equations and eigenfunctions. Then, we presented the numerical solutions of the eigenvalue equations. When the depth of the parabolic potential increases the eigenenergies of

the ground and first few excited states decrease to more negative values as shown in Table II. By plotting the eigenfunctions of these low lying states we have realized that as the eigenenergies decrease the numerical solutions become instable. Therefore, in Section III, we applied JWKB approximation to check the validity of the numerically found eigenvalues. The results in Tables I-II show that the JWKB approximation and the numerical solution for the eigenenergies agree very well except in the transition region of the potential given in Eq. (2). So, we conclude that one can use JWKB approximation to find the eigenvalues for this potential when the numerical solutions fail.

In section IV, we obtained the formula for the transition amplitudes and found the transition probabilities from the ground and second excited eigenstates of the harmonic trap to the ground state of the harmonic trap with a dimple described by the truncated parabolic potential for different dimple depths, using the sudden perturbation theory. In the following studies we aim to use these and similar results in three dimensions for modeling the sudden turn on of dimple potential experiments [4].

In section V, we have first shown that the truncated parabolic function provides a representation of the Dirac δ function. Moreover, we have also demonstrated that the bound state spectrums of the potentials given in Eqs. (33) and (2) reduce to the spectrum of the Dirac δ potential and harmonic potential with a Dirac δ as $a \rightarrow 0$, for fixed U_0a . As one can see from the Bose-Einstein distribution $\langle n_i \rangle = 1/(e^{\beta(E_i - \mu)} - 1)$ for a non-interacting Bose gas the effect of the trapping potential to the thermodynamic properties of the gas comes only through the eigenvalues of the potential. So, we come to the following conclusion: The fact that the eigenvalues of the truncated parabolic potential reduce to the eigenvalues of the Dirac δ potential in the limit $a \rightarrow 0$, for fixed U_0a , shows that the results obtained modeling the dimple potential with a Dirac δ for a non-interacting Bose-Einstein condensate in a harmonic trap with a dimple [12, 13] is included in the parabolic model of the dimple as a special case.

Acknowledgments

MÇA and HU acknowledge the support by TUBITAK (Project No:108T003). We also thank gratefully to Fatih Erman for useful discussions.

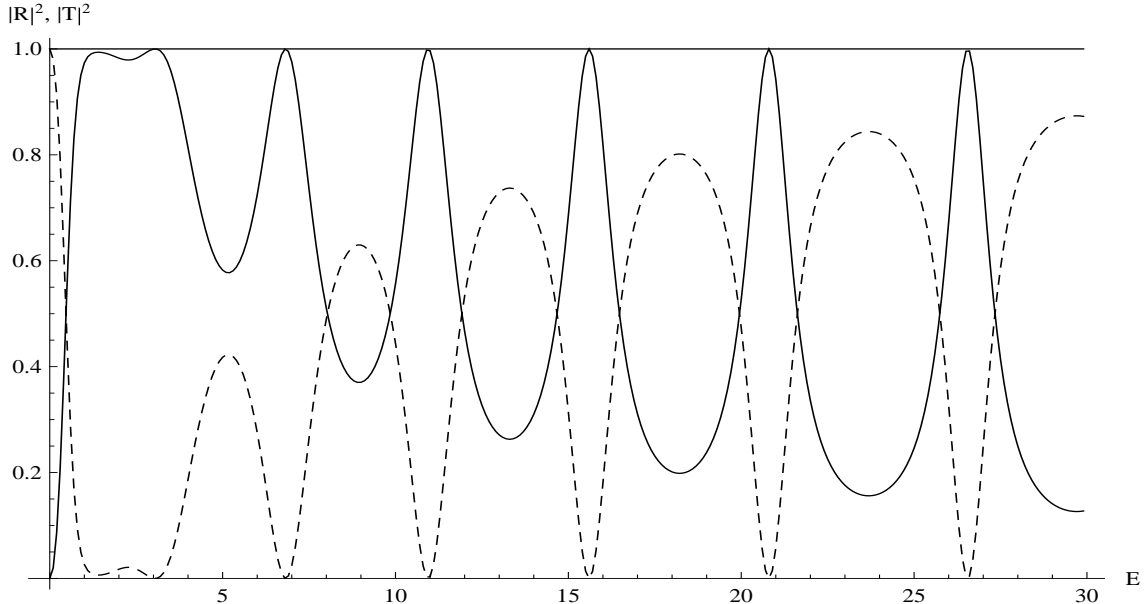


FIG. 3: The change of the tunneling and reflection probabilities $|T|^2$ and $|R|^2$ for the truncated parabolic potential, Eq. (33), with increasing energy of the incoming wave and for fixed $a = 3$, $U_0 = 10$ in natural units. The solid and dashed lines represent $|T|^2$ and $|R|^2$, respectively.

VII. APPENDIX

We present in this appendix, the change of the tunneling and reflection probabilities with respect to energy E of the incoming wave, width a and depth U_0 of the potential given in Eq. (33). The scattering wave function, reflection (R) and tunneling (T) amplitudes for this potential is given in Eqs. (43), (48) and (51), respectively. We first present the change of the tunneling and reflection probabilities with increasing energy E of the incoming wave in Fig. 3, for fixed potential width $a = 3$ and depth $U_0 = 10$. Here we use natural units $\hbar = 1$, $m = 1/2$. One can see from the Fig. 3, as E increases from zero, the tunneling probability first increases almost up to certainty. However, then it begins to oscillate with increasing amplitudes and widths such that local maximums are unity. Although the local minimums of these oscillations decrease almost up to zero, they never become equal to zero up to $E = 1000$.

Then, in Fig. 4, we show the variation of the tunneling and reflection amplitudes for increasing a and fixed $U_0 = 10$, $E = 1$. We see that the tunneling probability oscillates such that local maximums touch one and as a increases the amplitude of the oscillations

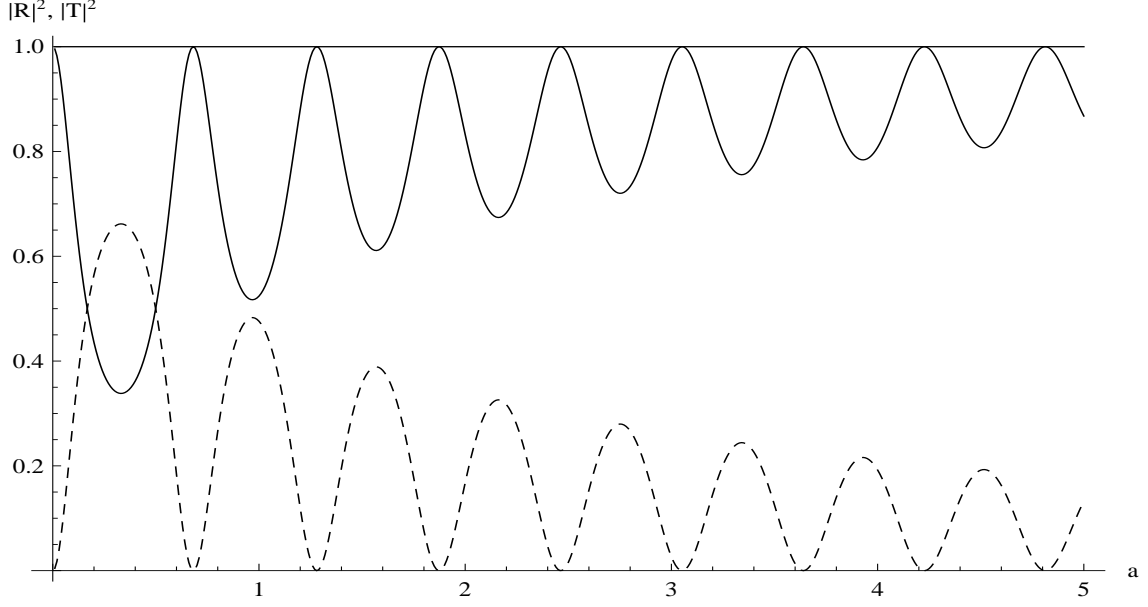


FIG. 4: The change of $|T|^2$ and $|R|^2$ for the truncated parabolic potential, Eq. (33), with increasing potential width a and for fixed $E = 1$, $U_0 = 10$ in natural units. The solid and dashed lines represent $|T|^2$ and $|R|^2$, respectively.

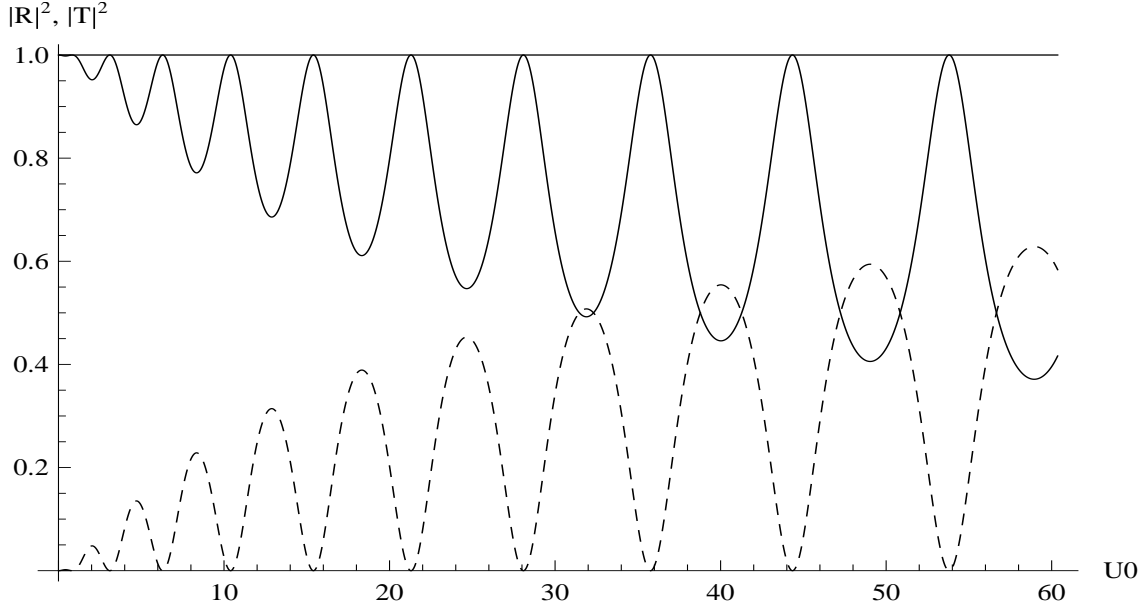


FIG. 5: The change of $|T|^2$ and $|R|^2$ for the truncated parabolic potential, Eq. (33), with increasing potential depth U_0 and for fixed $E = 1$, $a = 3$ in natural units. The solid and dashed lines represent $|T|^2$ and $|R|^2$, respectively.

decrease. Finally, we demonstrate the change of the $|T|^2$ and $|R|^2$ for increasing U_0 but for

fixed $E = 1$ and $a = 3$ in Fig. 5. Similar to the case of varying E , with increasing U_0 , $|T|^2$ oscillates with increasing amplitudes where local maximums are again one.

-
- [1] P.W. Pinkse, A. Mosk, M. Weidemler, M.W. Reynolds, T.W. Hijmans, J.T.M. Walraven, Phys. Rev. Lett. 78 (1997) 582.
 - [2] D.M. Stamper-Kurn, H-J. Miesner, A.P. Chikkatur, S. Inouye, J. Stenger, W. Ketterle, Phys. Rev. Lett. 81 (1998) 2194.
 - [3] Z-Y. Ma, C.J. Foot, S.L. Cornish, J.Phys. B. 37 (2004) 3187.
 - [4] M.C. Garrett *et all*, Phys. Rev. A. 83 (2011) 013630.
 - [5] D. Jacob, E. Mimoun, L. De Sarlo, M. Weitz, J. Dalibard, F.Gerbier, New J. Phys. 13 (2011) 065022.
 - [6] M. Hammes, D. Rychtarik, H.-C. Nägerl, R. Grimm, Phys. Rev. A 66 (2002) 051401.
 - [7] I. Bloch, J. Dalibard, W. Zwerger, Rev. Mod. Phys. 80 (2008) 885.
 - [8] A. Görlitz *et all*, Phys. Rev. Lett. 87 (2001) 130402.
 - [9] H. Ott, J. Fortagh, Schlotterbeck G., A. Grossmann, C. Zimmermann, Phys. Rev. Lett. 87 (2001) 230401.
 - [10] B.K. Teo, G. Raithel, Phys. Rev. A. 65 (2002) 051401(R).
 - [11] K. Günter, T. Stöferle, H. Moritz, M. Köhl, T. Esslinger, Phys. Rev. Lett. 95 (2005) 230401.
 - [12] H. Uncu, D. Tarhan, E. Demiralp, O. E. Mustecaplioglu, Phys. Rev. A. 76 (2007) 013618.
 - [13] J. Goold, D. O'Donoghue, Th. Busch, J. Phys. B: At. Mol. Opt. Phys. 41 (2008) 215301.
 - [14] A.D. Atkinson, W.H. Crater, Am.J.Phys 43 (1975) 301.
 - [15] M.P. Avakian, G.S. Pogosyan, A.N. Sissakian, V.M. Terontanyan, Phys. Lett. A 124 (1987) 233.
 - [16] E. Demiralp, J.Phys.A: Math. Gen. 38 (2005) 4783.
 - [17] X. Wang, L.-H. Tang, R.-L. Wu, N. Wang, Q.-H. Liu, Commun. Theor. Phys 53 (2010) 247.
 - [18] E. Demiralp, H. Beker, J. Phys. B. 36 (2003) 7449.
 - [19] M. Gadella, M.L. Glasser, L.M. Nieto, Int. J. Theor. Phys. 50 (2011) 2144.
 - [20] J.J. Álvarez, M. Gadella, L.M. Nieto, Int. J. Theor. Phys. 50 (2011) 2161.
 - [21] H. Erkol, E. Demiralp, Phys. Lett. A 365 (2006) 55.
 - [22] H. Erkol, E. Demiralp, Mol. Phys. 107 (2009) 2053.

- [23] B. Sahu, B.Sahu, Phys. Lett. A 373 (2009) 4033.
- [24] N. N. Lebedev, Special functions and their applications, Prentice Hall Inc., New Jersey, 1965.
- [25] H. Jeffreys, Proc. London Math. Soc., 23 (1923) 428.
- [26] A.K. Ghatak ,R.L. Gallawa, I.C. Goyal, Modified Airy Functions and WKB Solutions to the Wave Equation, NIST, Washington 1991.
- [27] M. Huruska, W.-Y. Keung, U. Sukhatme, Phys. Rev. A 55 (1997) 3345.
- [28] L.D. Landau, E.M. Lifshitz, Quantum Mechanics, Butterworth Heinemann, Oxford, 1977.
- [29] L.I. Schiff, Quantum Mechanics, McGraw-Hill, New York, 1968.
- [30] D.M. Stamper-Kurn, H.-J. Miesner, A.P. Chikkatur, S. Inouye, J. Stenger, W. Ketterle, Phys. Rev. Lett. 81 (1998) 2194.
- [31] C. Cohen-Tannoudji, B. Diu, F. Laloë, Quantum Mechanics Vol:2, Hermann, Paris, 1977.
- [32] E.F. Hoskins, Delta Functions , Horwood Publishing, Sussex, 1999.
- [33] We use Mathematica for the numerical solutions of the Eq. (15) and (16).
- [34] The JWKB approximation is called as WKB approximation in most physics books. However the mathematical formalism is introduced by H. Jeffreys [25] so we call it JWKB approximation.
- [35] The fact that $H_1(x)$, $H_2(x)$ and $H_3(x)$ are not unique do not affect the result.
- [36] Since we take U_0a is equal to a constant c , $\nu = \sqrt{2U_0/(ma^2)}$ becomes $\nu = \sqrt{2c/(ma^3)}$. Hence ν is of order $a^{-3/2}$.

TABLE II: The eigenenergies of low lying eigenstates for $\omega = 2\pi 20\text{Hz}$, $m = 23 \text{ amu}$, $a = 11\mu\text{m}$, $U_0 = 1.0 \cdot 10^{-30} \text{ J}$ and \hbar is in SI units. For these values $n' = 15$ and $V(a) = 2.75 \hbar\omega$. All the energies are in units of $\hbar\omega$.

The Eigenenergies				
	The Eigenstate No	Analytic	JWKB	Difference (Analytic-JWKB)
$E_n^{(1)}$	0	-72.7948	-72.7948	0.0000
	1	-67.4650	-67.4650	0.0000
	2	-62.1353	-62.1353	0.0000
	3	-56.8055	-56.8055	0.0000
	4	-51.4758	-51.4758	0.0000
	5	-46.1461	-46.1461	0.0000
	6	-40.8163	-40.8163	0.0000
	7	-35.4866	-35.4866	0.0000
	8	-30.1570	-30.1569	0.0001
	9	-24.8278	-24.8271	0.0007
	10	-19.5005	-19.4974	0.0031
	11	-14.1807	-14.1676	0.0131
	12	-8.8874	-8.8379	0.0495
	13	-3.6816	-3.5082	0.1734
	14	1.2167	1.8216	0.6049
$E_n^{(2)}$	15	4.8125	4.4790	0.3335
	16	6.0940	6.0210	0.0730
	17	7.3188	7.4137	0.0949
	18	8.8970	8.7300	0.1670
	19	9.8991	9.9980	0.0989
	20	11.3352	11.2316	0.1036
	21	12.4303	12.4396	0.0093
	22	13.6232	13.6273	0.0041
	\vdots	\vdots	\vdots	\vdots
	499	497.1836	497.1835	0.0001
	500	498.1856	498.1857	0.0001